SPECIAL MERRA COLLECTION

Warm Season Subseasonal Variability and Climate Extremes in the Northern Hemisphere: The Role of Stationary Rossby Waves

SIEGFRIED SCHUBERT

Global Modeling and Assimilation Office, NASA GSFC, Greenbelt, Maryland

HAILAN WANG*

Global Modeling and Assimilation Office, NASA GSFC, Greenbelt, and Goddard Earth Sciences and Technology Center, University of Maryland at Baltimore County, Baltimore, Maryland

MAX SUAREZ

Global Modeling and Assimilation Office, NASA GSFC, Greenbelt, Maryland

(Manuscript received 23 December 2010, in final form 4 April 2011)

ABSTRACT

This study examines the nature of boreal summer subseasonal atmospheric variability based on the new NASA Modern-Era Retrospective Analysis for Research and Applications (MERRA) for the period 1979–2010. An analysis of the June, July, and August subseasonal 250-hPa meridional v-wind anomalies shows distinct Rossby wave–like structures that appear to be guided by the mean jets. On monthly subseasonal time scales, the leading waves [the first 10 rotated empirical orthogonal functions (REOFs) of the 250-hPa v wind] explain about 50% of the Northern Hemisphere v-wind variability and account for more than 30% (60%) of the precipitation (surface temperature) variability over a number of regions of the northern middle and high latitudes, including the U.S. northern Great Plains, parts of Canada, Europe, and Russia. The first REOF in particular consists of a Rossby wave that extends across northern Eurasia where it is a dominant contributor to monthly surface temperature and precipitation variability and played an important role in the 2003 European and 2010 Russian heat waves. While primarily subseasonal in nature, the Rossby waves can at times have a substantial seasonal mean component. This is exemplified by REOF 4, which played a major role in the development of the most intense anomalies of the U.S. 1988 drought (during June) and the 1993 flooding (during July), though differed in the latter event by also making an important contribution to the seasonal mean anomalies. A stationary wave model (SWM) is used to reproduce some of the basic features of the observed waves and provide insight into the nature of the forcing. In particular, the responses to a set of idealized forcing functions are used to map the optimal forcing patterns of the leading waves. Also, experiments to reproduce the observed waves with the SWM using MERRA-based estimates of the forcing indicate that the wave forcing is dominated by submonthly vorticity transients.

1. Introduction

The boreal summer extratropical circulation lacks the strong jets and large-amplitude stationary waves that typify the boreal winter climate. This, together with the presence of pervasive tropical easterlies that inhibit remote forcing from the tropics, tends to limit boreal summer middle-latitude variability to more local/regional processes, with mesoscale convective weather systems and land–atmosphere coupling playing important roles (e.g., Parker and Johnson 2000; Koster et al. 2000). Nevertheless, the summer season does exhibit substantial variability on monthly time scales including periods of extreme heat and flooding that at times appear to develop as part of continental- or even planetary-scale circulation changes (e.g., Carril et al. 2007). The nature of such large-scale summer circulation changes, including

* Current affiliation: Science Systems and Applications, Inc., Lanham, Maryland.

Corresponding author address: Siegfried Schubert, 8800 Greenbelt Rd., NASA GSFC, Greenbelt, MD 20771.
E-mail: siegfried.d.schubert@nasa.gov

DOI: 10.1175/JCLI-D-10-05035.1

© 2011 American Meteorological Society

the mechanisms that act to maintain them on time scales far longer than those of local weather processes, is as yet unclear. One potentially important mechanism is Rossby wave propagation, in which the jet acts as a waveguide—a process known to be an important source of circumglobal teleconnectivity in winter (e.g., Hoskins and Ambrizzi, 1993; Branstator 2002).

While summer jets in the upper troposphere are weaker than the typical winter jets, there is now considerable evidence that the meridional gradients and nearly circumpolar extent of the summer jets can result in important guides for Rossby waves. Ambrizzi et al. (1995) summarized the teleconnectivity associated with the boreal summer waveguides and preferred propagation patterns toward and away from the waveguides. Newman and Sardeshmukh (1998) examined the seasonality of the Pacific–North American response to remote low-frequency forcing and showed that the changes are tied to the seasonal changes in the shape and location of the Rossby waveguide. They further showed that the amplitude of the forced response over the United States to forcing over the west Pacific can be larger in June than any other month of the year.

In this study, we take a new look at the large-scale controls of boreal summer [June, July, and August (JJA)] surface temperature and precipitation variability on subseasonal (30–90 day) time scales using the output from the Modern-Era Retrospective Analysis for Research and Applications (MERRA) (Rienecker et al. 2011). The study builds on the results of a number of earlier studies that found that summertime Rossby waves have played an important role in summer climate extremes. For example, Namias (1983; 1991) found that some warm season droughts over the U.S. Great Plains such as the one that occurred in 1988 tend to be associated with upper-level anticyclones linked to standing Rossby wave patterns. Lyon and Dole (1995) showed that both the 1980 and 1988 droughts were associated with anomalous stationary wave patterns, with apparent source regions in the North Pacific. Chen and Newman (1998) suggested that the intense anomalous anticyclones associated with the 1988 drought were linked to propagating Rossby waves originating in the west Pacific. Liu et al. (1998) used a linear stationary wave model to show that diabatic heating and transients played an important role in the development of the seasonal mean circulation anomalies associated with the 1988 drought, while vorticity transients dominated the forcing of the circulation anomalies associated with the1993 flood. Lau and Weng (2002) and Lau et al. (2004) found that summertime precipitation anomalies over North American and the Asian monsoon regions appear to be linked by wave train patterns that recur on seasonal to interannual time scales.

Ding and Wang (2005) isolated an interannually varying Northern Hemisphere circumglobal teleconnection (CGT) pattern linked to the Indian monsoon. They found that the CGT has a preferred wavenumber-5 structure, is primarily confined within the waveguide associated with the NH summer jet stream, and is linked to significant rainfall and surface air temperature anomalies in the continental regions of western Europe, European Russia, India, east Asia, and North America. They suggested that the heat sources associated with the Indian summer monsoon may be responsible for maintaining the CGT. Ding and Wang (2007) further showed that such a CGT also operates on intraseasonal time scales. Jiang and Lau (2008) found evidence for an intraseasonally varying wave train extending from the western North Pacific to North America along a great circle path that links North American monsoon variability to that in the western North Pacific. Wang et al. (2010) found that the abnormally wet conditions in the Central Intermountain West of the United States during June 2009 were associated with a circumglobal teleconnection pattern, which they characterized as a short Rossby wave train along the jet stream waveguide with a wavenumber-5 structure.

In this study we look more generally at the characteristics of the boreal summer Rossby waves, using MERRA to quantify their structure and their impacts on surface meteorology on subseasonal time scales. A stationary wave model (SWM) is used to characterize the preferred regions of forcing of the leading waves and provides insights into the nature of the forcing terms. Section 2 describes the data and our diagnostic approach. The results of our diagnostic analysis are presented in section 3. Section 4 describes the results of the SWM experiments with idealized and MERRA-based estimates of the forcing. The summary and conclusions are given in section 5.

2. The data and diagnostic approach

The analysis is based on MERRA (Rienecker et al. 2011). MERRA was produced with the Goddard Earth Observing System Data Assimilation System version 5 (GEOS-5) documented in Rienecker et al. (2008), consisting of the GEOS-5 atmospheric model and the Gridpoint Statistical Interpolation (GSI) analysis system, the latter being a system jointly developed by the Global Modeling and Assimilation Office (GMAO) and National Oceanic and Atmospheric Administration (NOAA)'s National Centers for Environmental Prediction. The GEOS-5 assimilation system includes an incremental analysis update (IAU) procedure (Bloom et al. 1996) that slowly adjusts the model states toward the observed state. This has the benefit of minimizing any unrealistic spindown (or spinup) of the water cycle. MERRA was run at a resolution of ½° latitude × ⅔° longitude with 72 levels extending to 0.01 hPa. More information about MERRA can be found on the Web site

(http://gmao.gsfc.nasa.gov/research/merra/). This study uses standard monthly mean (JJA) and hourly output that is provided on 42 pressure levels at a horizontal resolution of 1° latitude × 1.25° longitude for the period 1979–2010.

In addition to MERRA, we make use of other observations consisting of the monthly mean (2.5° latitude by 2.5° longitude) Global Precipitation Climatology Project (GPCP, version 2) precipitation data documented in Adler et al. (2003), and the Climate Research Unit (CRU) monthly mean surface air temperature product (Mitchell and Jones 2005). The CRU temperatures (version TS3.0) are on a spatial grid of 0.5° latitude by 0.5° longitude.

The leading patterns of 250-hPa meridional v-wind subseasonal variability of monthly means are isolated using rotated empirical orthogonal functions (REOFs), where varimax rotation (e.g., Richman 1986) is used to help separate (geographically) the leading wave structures. After some experimentation, we found that rotating the first 60 EOFs produces stable results (rotating more than that has no effect on the leading REOFs). The connections between these patterns of variability and other fields (e.g., precipitation and surface air temperature) are determined using both correlations and linear regression. While our choice of using the v wind is somewhat arbitrary, we did find that the v wind is particularly well suited for emphasizing the wavy component of the middle-latitude flow, and the REOFs provide a very clean depiction of the Rossby waves and their relationship to the jets. It turns out that the REOFs based on the 250-hPa height field (not shown) show similar features, although the leading REOFs show a somewhat more complex spatial structure including a greater zonal component for some of the patterns.

The statistical significance of the correlations and regressions is determined using a Monte Carlo approach that mimics the calculations done with the data. For the correlations, we first generate two sets of 96 (3 months times 32 years) independent, identically distributed (iid) normal random variates with zero mean and unit variance. Then, ''intraseasonal'' anomalies are computed by removing the average of every set of three iid variates. Next, the correlations between the two sets of anomalies are computed. These steps are repeated 1000 times and the resulting correlations are ordered from smallest to largest. The 25th and 975th values determine the 5% significance levels. For the regressions, the iid variates are scaled to have the same variance as the leading REOFs, and these are then used as the predictors for either precipitation or surface temperature at each grid point. This is carried out 1000 times (for every grid point) and the values are sorted from smallest to largest. The 950th (900th) value is the 5% (10%) significance value for each surface temperature (precipitation) regression.

3. Diagnostic analysis based on MERRA

In this section, we examine the variability of the upper-tropospheric circulation on subseasonal time scales for the months of JJA for the years 1979–2010. This includes an assessment of the extent to which the circulation changes are linked to surface temperature and precipitation variability. We begin by focusing on the 250-hPa v-wind field—a quantity that provides a clear measure of upper-tropospheric wave activity.

Figure 1 shows examples of the spatial structure and time evolution of subseasonal wind variability based on lag correlations of the 250-hPa v wind with respect to three different base points. The results are based on daily fields that have been bandpass (30–90 day) filtered using a symmetric, 4-pole, low-pass tangent-Butterworth filter (Oppenheim and Schafer 1975). When the base point is located in the central Great Plains, the correlations (at lag zero) show a clear signature of a standing wave that spans much of the western hemisphere and is largely embedded within the jet stream with a zonal wavenumber-6 structure. An examination of the time lags reveals that energy is moving through the wave from west to east with a group velocity of 20–25 m s^{-1}. Similar results are obtained without filtering (not shown), although the far-field components of the wave are obscured by the presence of higher-frequency waves and the spatial scale is slightly smaller, due to mixing with the shorter spatial scales of the high frequency waves.

The results for a base point over northwestern Russia (middle panels) show a somewhat different behavior, although the wave again has a fixed phase. In this case, the wave energy moves along the North America–Atlantic jet, but then appears to split at the jet exit region, with most of the wave activity moving northeastward out of the jet in a path over northern Eurasia (north of the jet) where it has a zonal wavelength of about 90° longitude. Some of the wave energy moves south and east (initially south over northern Africa), remaining effectively embedded in the Asian jet. The behavior is again similar in the unfiltered data (not shown). The right panels show the structure obtained if the base point is moved south over the Caspian Sea. In that case the wave energy is almost entirely confined to the jet, with the wave extending from Europe across southern Eurasia into the Pacific.

The above results are representative of the structures and evolution obtained using different base points throughout the hemisphere in or near the jets, with most base points showing the wave activity confined to the jet (e.g., left panels of Fig. 1). The main exceptions are the base points near the jet exit region over the North Atlantic where some if not most of the energy appears to propagate out of and to the north of the jets (e.g., middle panels of Fig. 1).

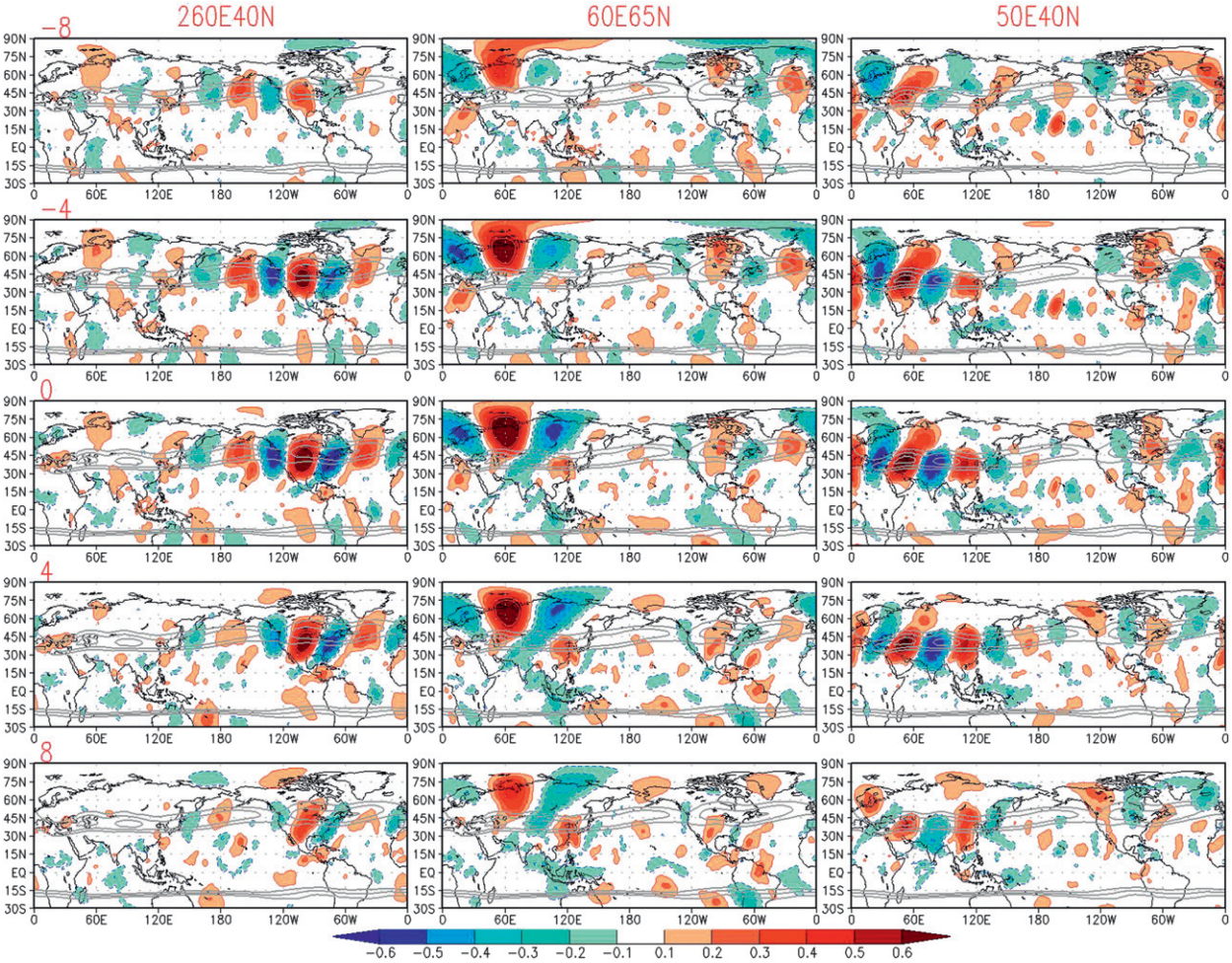

FIG. 1. Lag correlations [(top to bottom) −8, −4, 0, 4, and 8 days] of the MERRA 30–90-day-filtered 250-hPa v wind for JJA of 1979–2010. The correlations are with respect to 250-hPa wind v-wind indices at (left) 40°N, 260°E, (middle) 65°N, 60°E, and (right) 40°N, 50°E. The thick gray contours show the long-term JJA mean (1979–2010) 250-hPa u wind at 15, 20, 25 m s^{-1}.

We note that results based on a filter that retains 10–30 days (not shown) also show clear evidence of Rossby waves, although at these time scales the spatial scales are somewhat smaller and there is clear evidence of eastward phase propagation. We will discuss further the characteristics of the stationary Rossby waves in the next section in the context of a stationary wave model.

In the following, we focus the analysis on monthly mean quantities. Our estimate of subseasonal variability in that case is based on the monthly mean deviations from both the long-term mean for each month and the seasonal (JJA) mean for any particular year. In particular, the total monthly mean variance in V averaged over the summer (JJA) season can be decomposed as follows:

$$\overline{\langle (V-\overline{V})^2 \rangle} = \overline{\langle V' \rangle^2} + \overline{\langle V'^{*2} \rangle}, \qquad (1)$$

where the overbar denotes the long-term mean (1979–2010) for a particular month, and the prime is the deviation from the long-term mean. Also, the angle brackets denote a seasonal mean (JJA), and the star is the deviation from the seasonal mean. The first term on the right-hand side (rhs) is the interannual variance of the seasonal mean anomalies, while the second term on the rhs is the subseasonal variance—our main focus.

Figure 2 shows the unbiased estimates of both terms on the rhs of (1).[1] The results show the dominance of the subseasonal variance (top panel of Fig. 2), highlighting

[1] For the subseasonal variance, using an unbiased estimate is especially important since for each year there are only $N = 3$ terms in the sum of squares. The unbiased variance estimate for each year is obtained by dividing the sum of squares by $N - 1 = 2$. These are then averaged over 32 years.

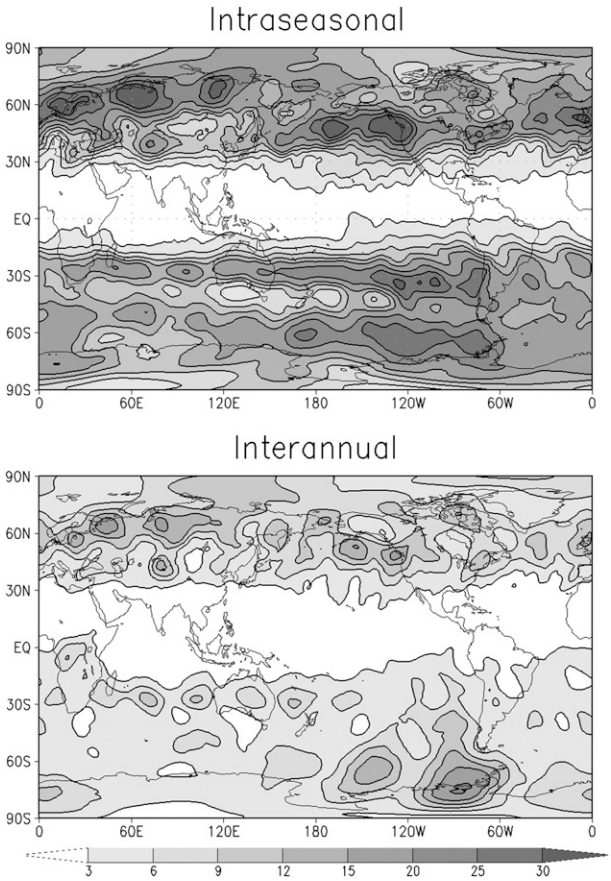

FIG. 2. Variance of the monthly mean 250-hPa v-wind anomalies for JJA for the period 1979–2010. The total seasonal mean monthly variance is decomposed into the (top) intraseasonal variance of monthly means and (bottom) interannual variance of the seasonal mean anomalies. See text for details. Units are $(\mathrm{m\ s^{-1}})^2$.

the importance of addressing the nature of these time scales for improving our understanding of boreal summer variability. While the focus here is on the Northern Hemisphere, we note that the Southern Hemisphere also shows extensive regions of high subseasonal variability spanning the globe at both 30° and 60°S, especially in the Pacific sector, consistent with an important role for Rossby waves (e.g., Ambrizzi et al. 1995). In the Northern Hemisphere, local maxima occur over the eastern North Atlantic, Northern Europe, the Ural Mountains, northeastern Russia (just west of the Verhoyansk Mountains), a region just south of the Aleutian Islands, and on both the west and east coasts of North America. There is some evidence of a secondary track of relatively high variance over southern Eurasia, with local maxima just west of the Caspian Sea and again just west of the Tian Shan Mountains near 70°E and 40°N. The latter was identified by Ding and Wang (2005) as a potentially important region of interannual variability associated with the circumglobal teleconnection pattern mentioned in the introduction. Consistent with their results, we also find that region to have substantial interannual variability (bottom panel of Fig. 2). In general, the interannual variance of the seasonal mean anomalies is a weaker version of the subseasonal variance, with a geographical distribution that, however, tends to be in quadrature with that of the subseasonal variance (maxima tend to fall to the east of the corresponding subseasonal maxima). This indicates that the interannual variability is not simply a statistical residual of the intraseasonal variance. The geographical distribution of the variance discussed above, does suggest that regions of high topography, and possibly land–sea contrasts, may play some role in anchoring the variance.

We next summarize the subseasonal 250-hPa v-wind variability using REOFs (Richman 1986). Our focus is on the mature stationary Rossby waves, so REOFs should provide a reasonable set of basis functions for isolating any preferred regional development of these waves. Together, the first 5 (10) REOFs explain ⅓ (½) of the monthly-mean subseasonal variance. The first REOF (Fig. 3) bears a striking resemblance to the lag–zero one-point correlation map shown in the middle panels of Fig. 1. The second REOF is centered on the North Pacific region linking Asia with North America, while the third is centered over the North Atlantic, linking North America and Europe. The fourth REOF is centered over North America and is approximately in quadrature with the third, while the fifth REOF spans the Asian continent where it is for the most part embedded in the Asian jet extending from Europe to the North American continent. We note that the fifth REOF bears some resemblance to the CGT found by Ding and Wang (2005) on interannual time scales. As we shall see (in Fig. 7), our analysis also indicates that this wave train has a significant interannual component. In addition, REOF 1 is very similar to the leading intraseasonal teleconnection pattern found by Ding and Wang (2007).

It is not clear to what extent the REOFs can be interpreted as distinct physical modes of variability—something that is difficult to determine by purely statistical measures especially for rotated EOFs (the percent variance explained indicates little separation in variance, ranging from 8.2% for the first to 4.1% for the fifth REOF). Some indication that the leading REOF patterns represent physical modes of variability is given by the fact that they have counterparts in lag correlation patterns such as those shown in Fig. 1. Also, we will show in the next section that very similar wave structures can be produced, by forcing a stationary wave model with localized vorticity or heat sources (e.g., Fig. 11). It is also worth noting that there is some suggestion of a phase locking of

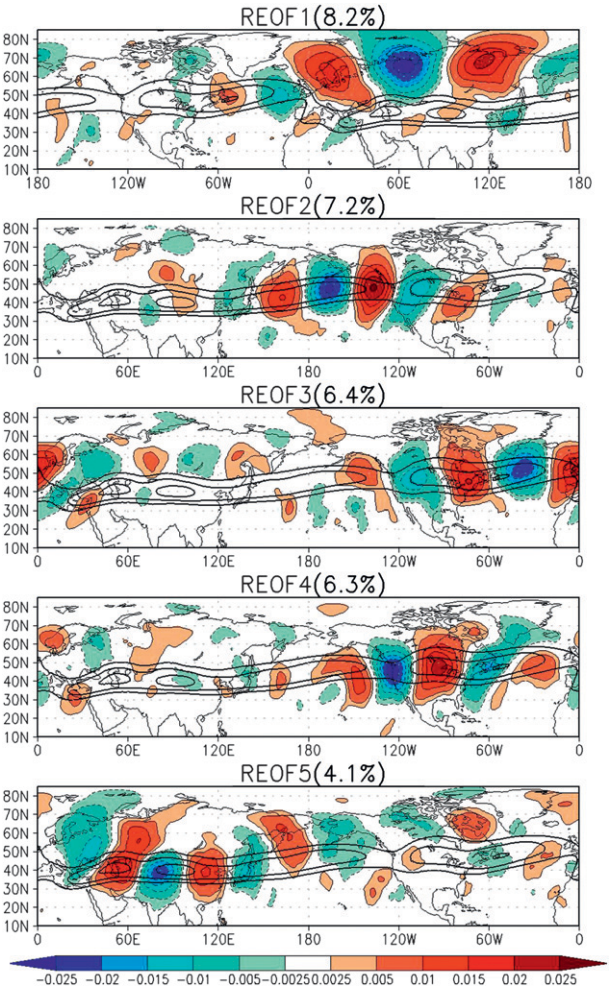

FIG. 3. The leading REOFs of the 250-hPa intraseasonal monthly mean v-wind anomalies for JJA of 1979–2010. Units are arbitrary. The thick black contours are the long-term JJA mean (1979–2010) 250-hPa u-wind at 15, 20, 25 m s^{-1}. Note that the central longitude in the plot for REOF 1 is 0°, while it is 180° for the others.

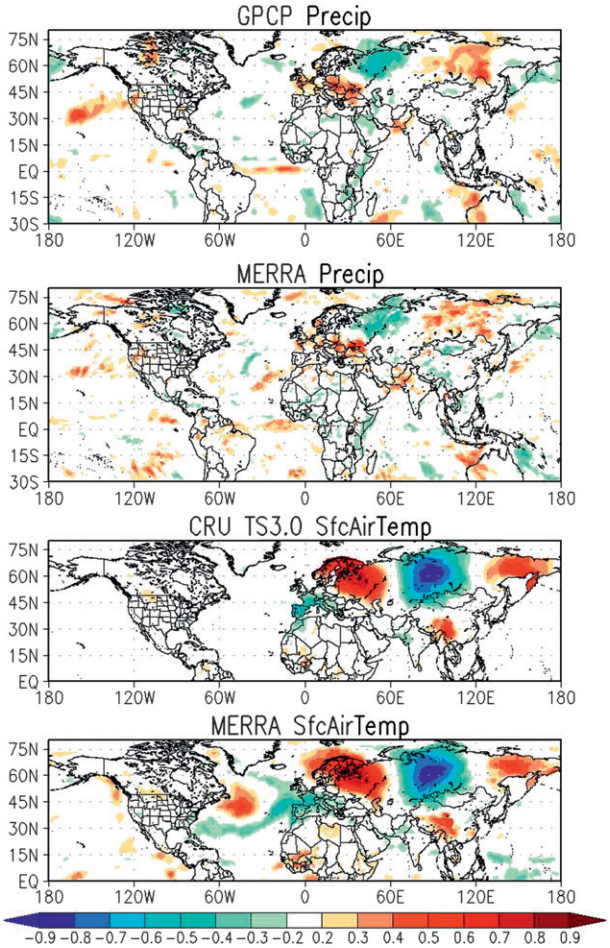

FIG. 4. The correlations between the first REOF of the 250-hPa subseasonal v-wind anomalies and subseasonal (a) GPCP precipitation, (b) MERRA precipitation, (c) CRU TS3.0 surface air temperature, (d) MERRA surface air temperature for JJA of 1979–2005. Note that 1979–2005 is the period that all the data are available. The contour interval is 0.1, starting at ±0.2. Absolute values >0.27 are significant at the 5% level based on a Monte Carlo test (see text).

the wave packets defined by the REOFs with the summertime stationary waves. In particular, REOFs 1 and 5 appear to develop in the North Atlantic trough and are distributed to the north and south of the Asian monsoonal high, respectively. REOF 2 coincides with the North Pacific oceanic trough, while REOFs 3 and 4 appear to emerge out of the North Pacific oceanic trough and extend across the North American (monsoonal) anticyclone into the North Atlantic trough.

While the leading REOFs are important contributors to the upper-tropospheric variability, it is not clear that they contribute in a significant way to subseasonal variability in surface meteorology. To examine this, we compute the correlations between the leading 250-hPa subseasonal v-wind REOFs [the associated rotated principal components (RPCs)] and subseasonal precipitation and surface temperature using both MERRA and independent observations. Figures 4 and 5 show examples of the correlations for REOF 1 and REOF 4, respectively. Correlations with absolute values greater than 0.27 are significant at the 5% level based on the Monte Carlo approach described in section 2. The results show, first of all, that MERRA provides very good estimates of both the temperature and precipitation variability, and in the case of the surface temperature provides information over the oceans that is not available from the gridded-station observations. These results give us confidence that we can also use MERRA to estimate the forcing of these waves (see next section).

The leading REOF is associated with a very distinctive pattern of precipitation and temperature correlations that

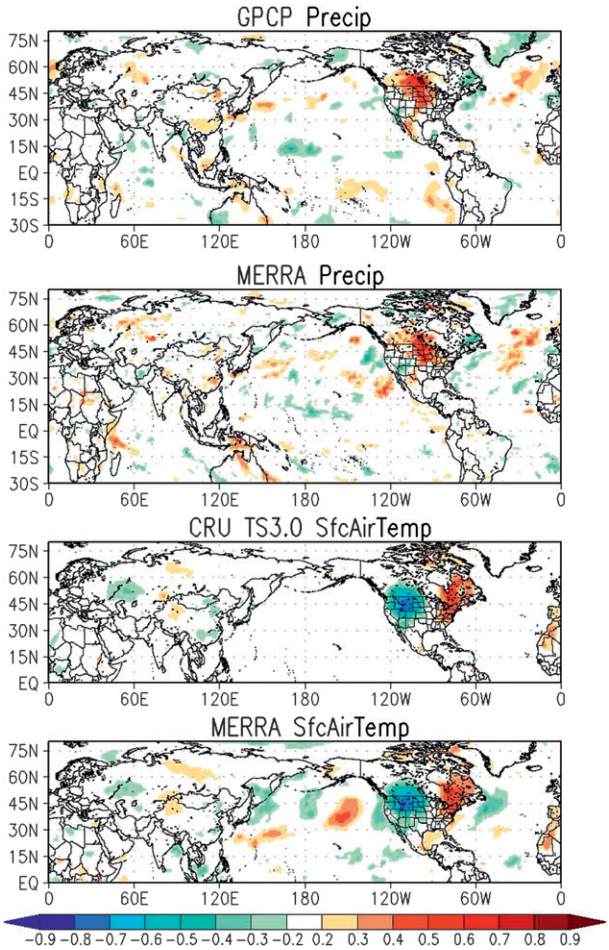

FIG. 5. As in Fig. 4, but for REOF4.

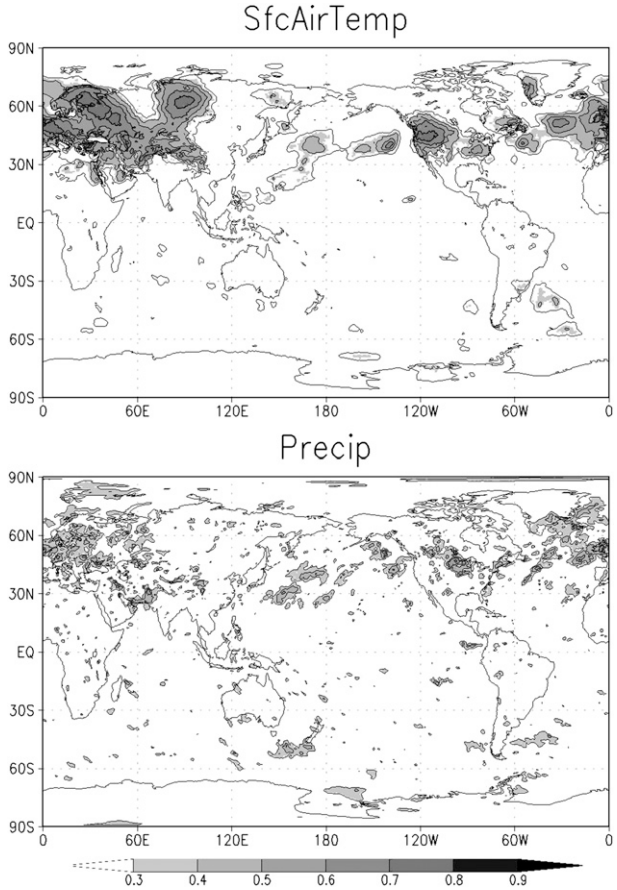

FIG. 6. The spatial distribution of the fraction of monthly (JJA—1979–2010) subseasonal variance of (top) surface air temperature and (bottom) precipitation explained by the first ten 250-hPa subseasonal v-wind REOFs, based on a linear regression. Contours start at 0.3 with a 0.1 interval. Shaded values are significant at the 5% (10%) level for temperature (precipitation) based on a Monte Carlo test (see text).

alternate in sign, extending across the Eurasian continent north of the jet, with precipitation correlations exceeding 0.3 in magnitude, while the magnitudes of the temperature correlations exceed 0.6 (Fig. 4). It is noteworthy that there are also significant precipitation correlations (exceeding 0.3) south of the Asian jet and significant temperature correlations over central China and parts of Northern Africa. The correlations associated with the fourth REOF (Fig. 5) are strongest over North America, with the largest precipitation correlations occurring in the U.S. northern Great Plains extending north into Canada. The temperature correlations have an east–west dipole with one pole centered over the Northern Great Plains and the other over eastern North America. The other leading REOFs also show significant temperature and precipitation correlations (not shown). REOF 2 is associated with a north–south wet–dry dipole over the United States and Canada, and an east–west dipole in temperature in the western and central United States. REOF 3 has significant temperature and precipitation correlations over eastern North America and Europe, and REOF 5 has significant precipitation and temperature correlations extending south and east from the Caspian Sea to India, parts of China, and Indonesia. While the details of the mechanisms by which the upper tropospheric waves impact the surface meteorology are beyond the scope of this paper, we note that the vertical structure of the waves (as determined from correlations with the v wind at 850 hPa—not shown) is largely barotropic, although there is some tendency for a westward tilt with height.

The impact of the leading REOFs on surface meteorology is summarized in Fig. 6 in terms of an explained variance based on a linear regression that uses the first 10 250-hPa u-wind REOFs as predictors. Shaded values are significant at the 5% (10%) level for surface temperature (precipitation) based on the Monte Carlo approach (see section 2). In the case of surface temperature,

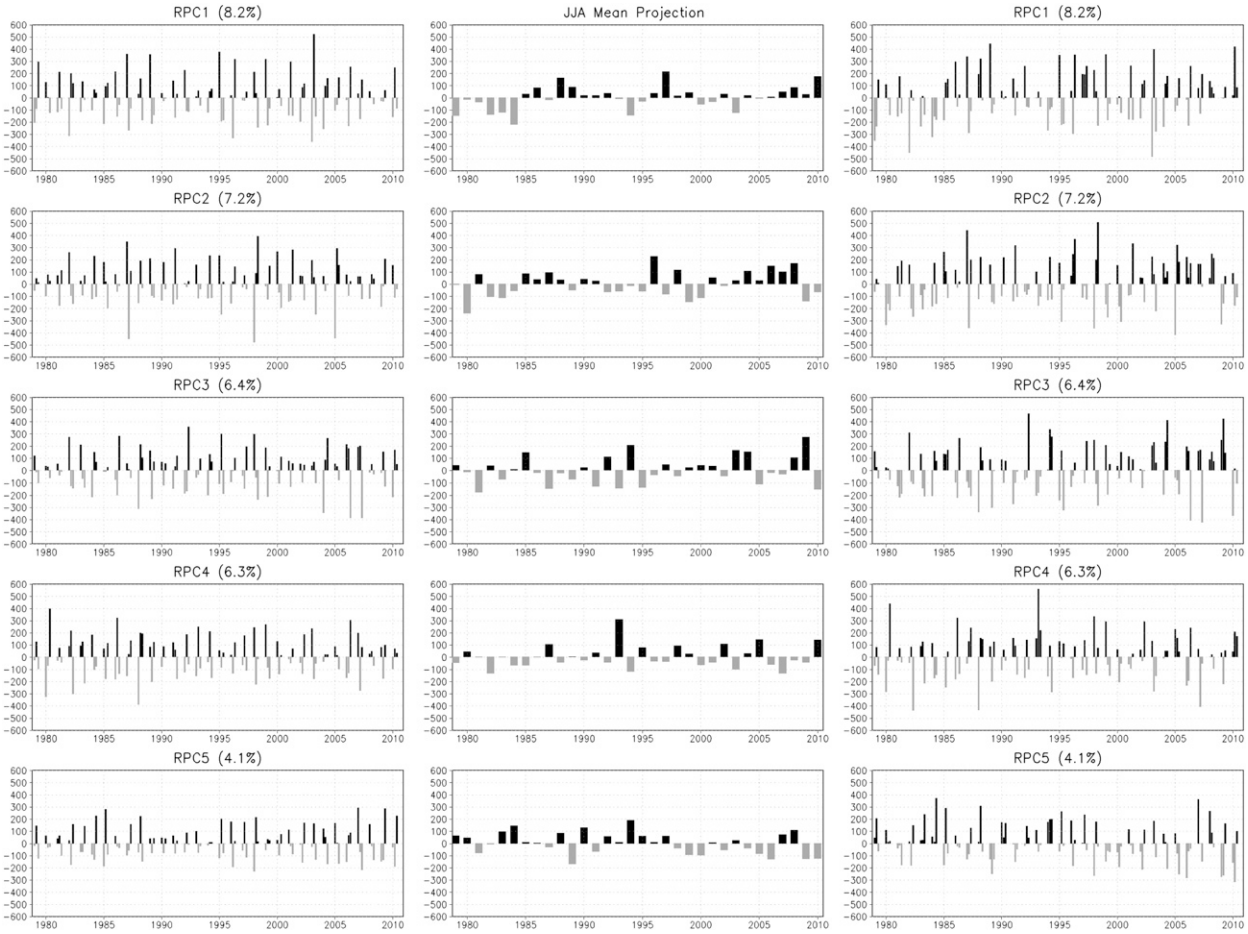

FIG. 7. (top to bottom) (left) The five leading RPCs of the 250-hPa subseasonal monthly mean v-wind anomalies for JJA of 1979–2010; (middle) the projection of the JJA seasonal mean 250-hPa v-wind anomalies onto the subseasonal REOFs; and (right) the sum of (a) and (b), equal to the projection of the full monthly 250-hPa v-wind anomalies onto the subseasonal REOFs.

the REOFs explain more than 60% of the monthly mean subseasonal variance over parts of northern Europe, Russia, and the western United States. In the case of precipitation, the explained variance is somewhat nosier and lower, although there are substantial regions in the North Atlantic, Europe, Russian, southern Eurasia, the North Pacific, and the United States and Canada where the explained variance exceeds 30%.

We next examine the time history of the RPCs to get a better sense of the character of the variability and to determine whether there are particular climate extremes that can be associated with one or more of the leading REOFs. Figure 7 (left panel) shows the 5 leading subseasonal RPCs for JJA of each year. The subseasonal variability shows little month-to-month persistence, although there is some tendency for extreme anomalies of one sign to be followed by a reversal in sign the following month—a result that is expected since the anomalies over a season must add to zero by design. Examples of extreme occurrences of the leading RPCs include the months of June and July of 2003 (RPC 1), June 1998 (RPC 2), and June 1988 (RPC 4). These are associated with the 2003 European heat wave, the spring–early summer 1998 flooding in the Midwest and northeast and drought to the south, and the 1988 U.S. summer drought.

Of course any particular monthly mean anomaly is potentially composed of both intraseasonal and interannual components as quantified in (1). We examine this here by projecting the seasonal mean anomalies onto the subseasonal REOFs.[2] The results (middle panels of Fig. 7) show that the leading subseasonal REOFs do at times have a substantial seasonal mean component, so that the total monthly variance associated with each REOF (right panels of Fig. 7) exhibits considerable month-to-month

[2] The calculation takes into account the fact that the REOFs are not spatially orthogonal.

persistence during some summers. A key example is the summer of 1993 when REOF 4 has a (positive) seasonal mean that dominates the total variance (Fig. 7–second row from bottom), so that the seasonal peak in July during the most intense flooding over the central United States, is a relatively smaller subseasonal fluctuation on top of the seasonal mean. This is in contrast with the summer of 1988, when REOF 4 has a relatively small seasonal mean component, and is instead characterized by a large subseasonal component dominated by a negative event during June of that year at the height of the drought. It is noteworthy that the drought event was much longer lived (extending into 1989) than the flood event. This underscores the basic subseasonal character of the waves that tend to be associated with the most intense (extreme) periods that occur in conjunction with what can be much longer-lived events dictated by other large scale forcing or feedbacks (see discussion at the end of this section).

We also see that the summer of 2003 was characterized by largely subseasonal variations in RPC 1 (top row of Fig. 7), in which the associated stationary Rossby wave changed sign from negative in June to positive in July and then back to negative in August. This reflects the subseasonal fluctuations in the 2003 heat wave over Europe, with the most intense heat occurring during June and early August, with a temporary relaxation of the heat wave during July (consistent with our expectations of the impact of REOF 1 on surface temperature shown in Fig. 4). In contrast, the 2010 heat wave over Russia is associated with a positive occurrence of REOF 1 that has a significant seasonal mean component, on top of a large-amplitude positive event that occurred during July—the peak of the Russian heat wave. This is again consistent with our expectations of the impact of REOF 1 on Russian surface temperature (Fig. 4).

Other noteworthy aspects of Fig. 7 include the large positive seasonal mean component of REOF 3 during 2009 associated with a very cool and wet summer extending from the Great Plains to the northeastern United States, and a large negative occurrence of RPC 2 in June 2005, associated with very dry conditions over Texas and record June rainfall in North Dakota. While there is no clear evidence of any trends in the seasonal means, there do appear to be extended periods where the REOFs have loadings of the same sign (e.g., REOFs 1 and 2—top two middle panels). There also appears to be a tendency toward more negative values in the loadings of REOF 5 after the mid-1990s (bottom middle panel of Fig. 7), though this is small compared to the month-to-month subseasonal variability.

Figures 8–10 provide examples of the important contributions made by the first and fourth REOFs to the monthly climate anomalies over Eurasia and North America. Here we have selected several months that have a substantial contribution from REOF 1 based on the RPC loadings shown in Fig. 7. The signature of REOF 1 is clearly evident in the 250 hPa v-wind anomalies (Fig. 8), with alternating positive and negative 250-hPa v-wind anomalies extending across northern Eurasia. It is noteworthy that most of the largest anomalies in REOF 1 occur during June. In fact, of the events exceeding two standard deviations in the subseasonal variability, four occurred in June, one in July, and none in August. The 2010 anomaly stands out because it occurs during July, and because it has a large seasonal mean component. That month is also distinguished by a large-amplitude southern track (embedded within the Asian jet waveguide) of the anomalies—in fact that aspect of the wave is associated with a large negative loading of REOF 5 (bottom right panel of Fig. 7).

Figure 9 shows the associated surface temperature anomalies. The anomalies are consistent with the signature of REOF 1 (cf. Fig. 4, bottom two panels). The alternating cold and warm surface temperature anomalies reflect the upper-level wind and associated height anomalies (with upper-level ridges associated with warm surface conditions over northern Eurasia). Particularly noteworthy are the warm anomalies over Europe during June 2003 and over eastern Russia during July 2010. In fact, during these two months the patterns of the surface temperature anomalies over Eurasia are particularly strongly linked with REOF 1. The spatial correlation (for the region 0°–120°E, 30°–80°N, land only) between the June 2003 (July 2010) temperature anomalies and the REOF 1 MERRA-based temperature correlation map shown in the bottom panel of Fig. 4 is equal to −0.81 (+0.72), respectively.[3] We note that the analogous spatial correlations for the precipitation anomalies (not shown) are −0.51 and +.35, for June 2003 and July 2010, respectively. Also during 2010, the southern track of the 250-hPa v-wind anomalies (Fig. 8) appears to be associated with cold (and wet—not shown) anomalies over northern Pakistan (also a signature of REOF 1—Fig. 4), which may have contributed to the intense flooding in that region in July and August. We note that REOF 5 also impacts that region, with the positive phase producing positive rainfall anomalies. In 2010, REOF 5 was negative in the early summer (associated with negative precipitation anomalies) and then switched to positive

[3] Here, we consider the temporal correlation maps (e.g., those shown in Figs. 4 and 5) as measuring the temperature (or precipitation) "fingerprints" of the upper-level REOFs. The spatial correlation between those correlation maps (or fingerprints) and the actual anomalies gives a measure of the contribution of the REOF in question to those anomalies.

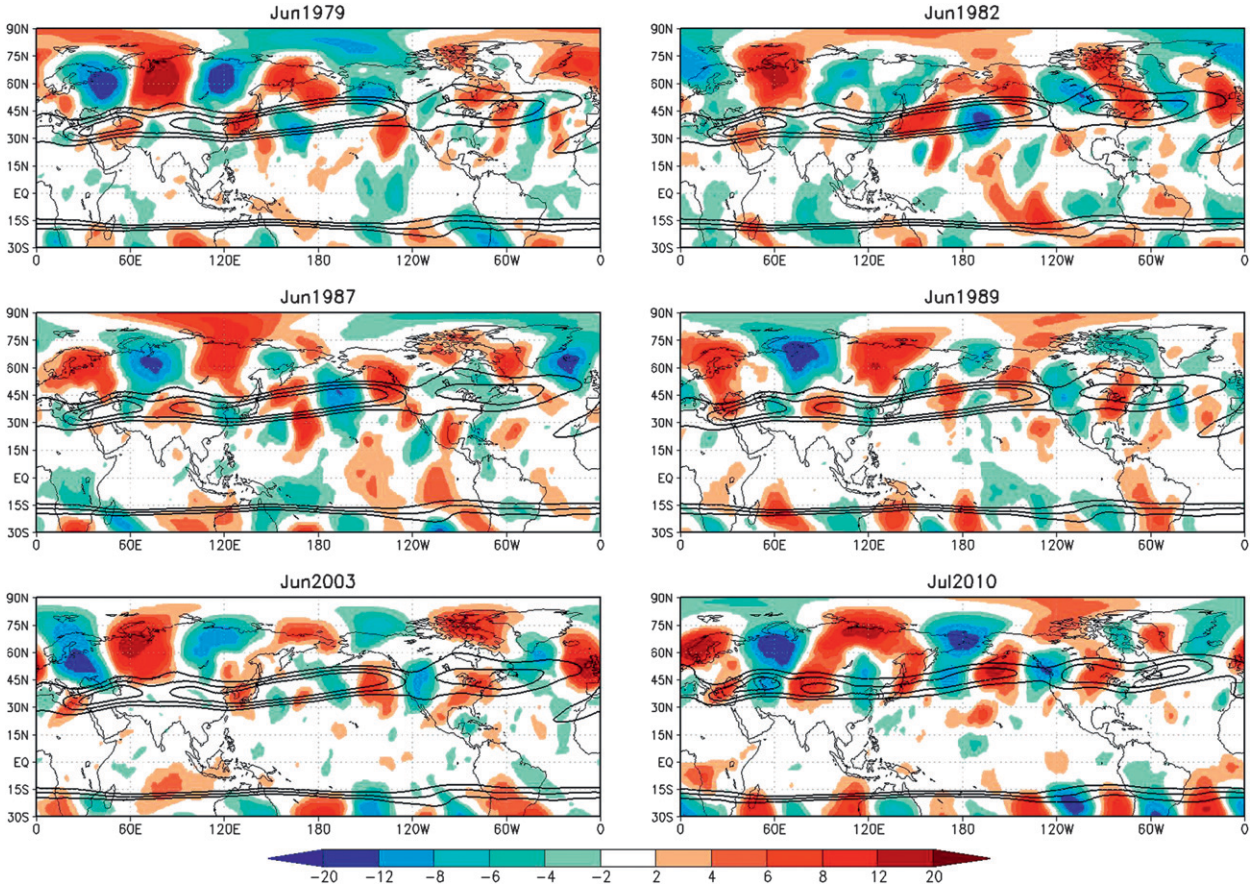

FIG. 8. The MERRA 250-hPa v-wind anomalies (deviations from the 1979–2010 monthly means) for selected months with a large amplitude in REOF 1 (see Fig. 7). REOF 1 had large negative values during June 1979, June 1982, and June 2003. It had large positive values during June 1987, June 1989, and July 2010. Units are m s^{-1}. Contours are the long-term mean (1979–2010) monthly 250-hPa u wind of 15, 20, 25 m s^{-1}.

values in August—presumably contributing to the flooding during that month.

Figure 10 shows the 250-hPa v-wind anomalies during the height of the July 1993 flooding and June 1988 drought over the United States and Canada. Also shown are the associated precipitation and surface temperature anomalies. The signature of REOF 4 is clearly evident in the 250-hPa v-wind anomalies during both months (positive in 1993 and negative in 1988). The precipitation and surface temperature anomalies during 1993 also have a clear signature of REOF 4 (cf. Fig. 5). The spatial correlation (for the region 22°–52°N, 65°–125°W, land only) between the July 1993 temperature (precipitation) anomalies and the REOF 4 MERRA-based temperature (precipitation) correlation map shown in the second (fourth) panel of Fig. 5 is equal to +0.85 (+0.56). In the case of the 1988 drought, the precipitation and surface temperature anomalies again show some signature of REOF 4; however, the anomalies are more widespread, consistent with an important contribution from land feedbacks as suggested by previous studies (e.g., Namias 1991; Atlas et al. 1993). In this case, the spatial correlation between the June 1988 temperature (precipitation) anomalies and the REOF 4 MERRA-based temperature (precipitation) correlation map is weaker, with a value of −0.59 (−0.38). In fact, Dirmeyer and Brubaker (1999) showed that while precipitation recycling reaches its maximum during the June peak of the 1988 drought, during the height of the 1993 floods in July, the recycling was considerably lower than during other months.[4]

We next turn to a stationary wave model to try to get a better understanding of the forcing and variability of the wave structures associated with the leading REOFs.

[4] Precipitation recycling is defined as the contribution of evaporation in a region to the precipitation in the same region.

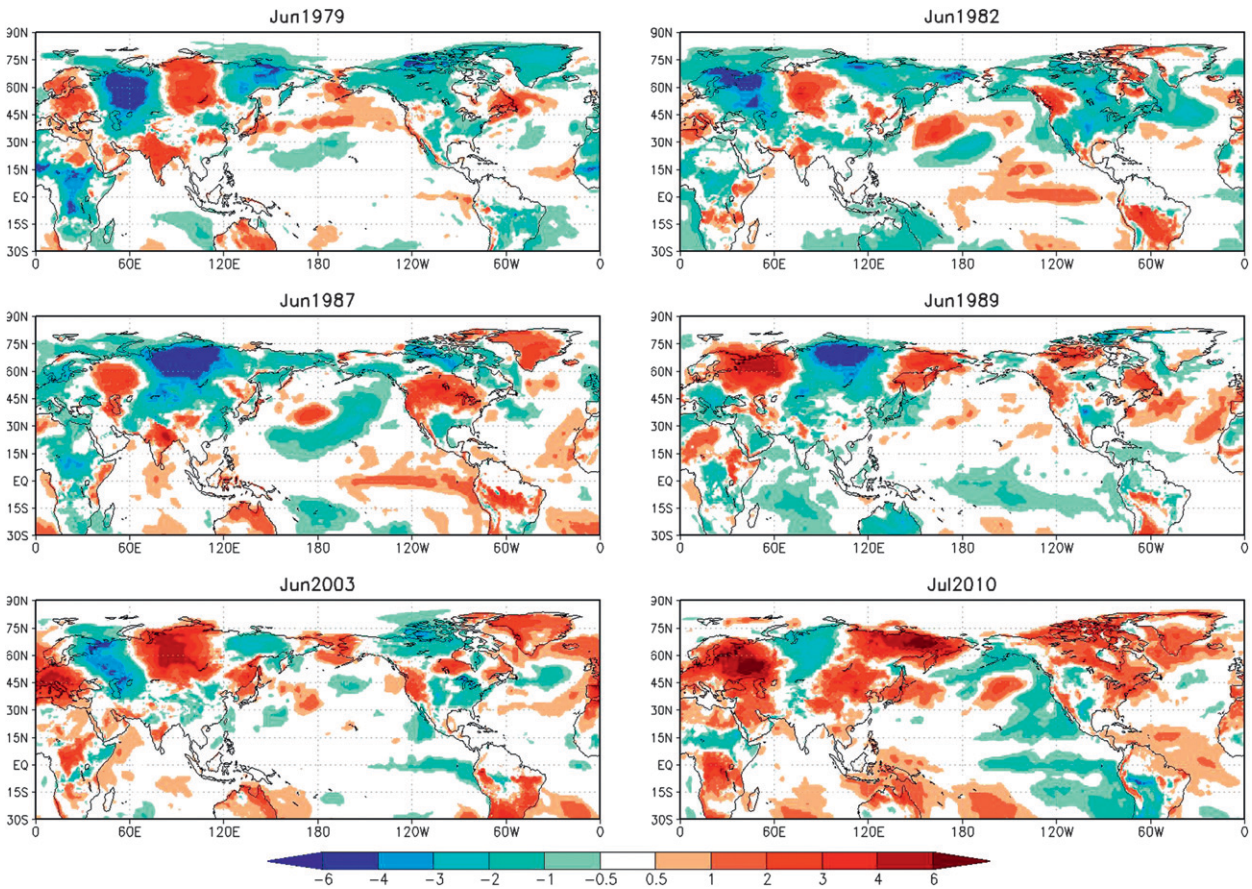

FIG. 9. As in Fig. 8, but for the MERRA surface air temperature anomalies. Units are °C.

4. Results from stationary wave model experiments

The SWM used in this study is the dry dynamical core of a full nonlinear time-dependent AGCM (Ting and Yu 1998). It is based on the three-dimensional primitive equations in σ coordinates. The model-generated transient disturbances are suppressed by strong damping. The model has rhomboidal wavenumber-30 truncation in the horizontal and 14 unevenly spaced σ levels in the vertical (R30L14). The SWM has been shown to be a valuable tool to diagnose the maintenance of both climatological and anomalous atmospheric circulation by evaluating the relative roles of stationary wave forcing over specific regions (e.g., Ting et al. 2001; Held et al. 2002; Lau et al. 2004). More details of the SWM can be found in Ting and Yu (1998).

In the experiments performed here, the background state for the SWM consists of the full three-dimensional climatological JJA flow computed from MERRA for the period 1979–2010. The stationary wave forcing consists of diabatic heating and transient flux convergences that are specified as idealized local forcing functions or estimated from MERRA daily output. We turn first to the idealized forcing experiments.

a. *Responses to idealized forcing*

The horizontal structure of the idealized forcing has a sine-squared functional form, with horizontal scales of 40° longitude by 10° latitude, and 10° longitude by 10° latitude for the diabatic heating and transient vorticity forcing, respectively. The vertical profiles of the idealized heating and transient vorticity forcing are defined following Fig. 13 of Liu et al. (1998). The heating profile has a maximum of 3 K day^{-1} in the middle troposphere, and the profile of the transient vorticity forcing has a maximum of 5.6×10^{-10} s^{-1} in the upper troposphere.

Figure 11 shows some examples of the response to idealized vorticity sources in selected locations. In the left panels the source is located just east of Japan. The response shows the development of a wave train embedded in the jet that extends eastward into North America. The wave train becomes fully developed with a zonal wavenumber-6 structure in about 30 days and resembles some of the wave trains found in MERRA (cf. REOF 2 in

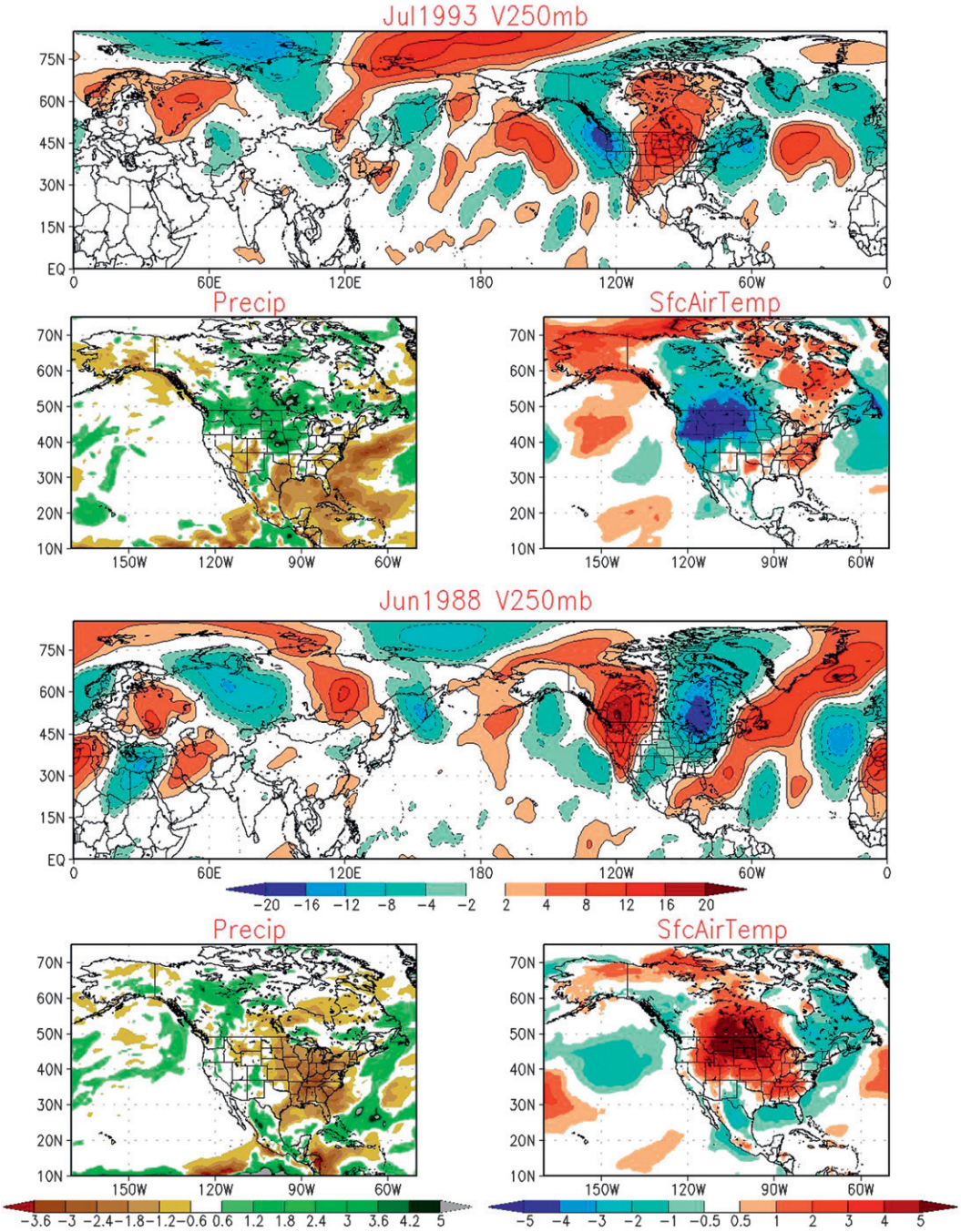

FIG. 10. (top) The MERRA 250-hPa v-wind anomalies (deviations from the 1979–2010 monthly means) for July 1993. (next row) The (left) MERRA precipitation and (right) surface air temperature anomalies during July 1993. (next row) The MERRA 250-hPa v-wind anomalies (deviations from the 1979–2010 monthly means) for June 1988. (bottom) The (left) MERRA precipitation and (right) surface air temperature anomalies during June 1988. The v-wind has units of m s^{-1}, precipitation has units of mm day^{-1}, and surface air temperature has units of °C.

Fig. 3). The middle panels of Fig. 11 show another example in which the source is placed in the eastern Pacific just south of the jet. In this case, the wave extends across North America and the Atlantic into Europe and is again largely embedded in the jet (cf. REOF 4 in Fig. 3). The panels on the right of Fig. 11 show an example where the source is placed slightly to the south of the North Atlantic jet exit region. In this case, the wave activity splits as it moves east

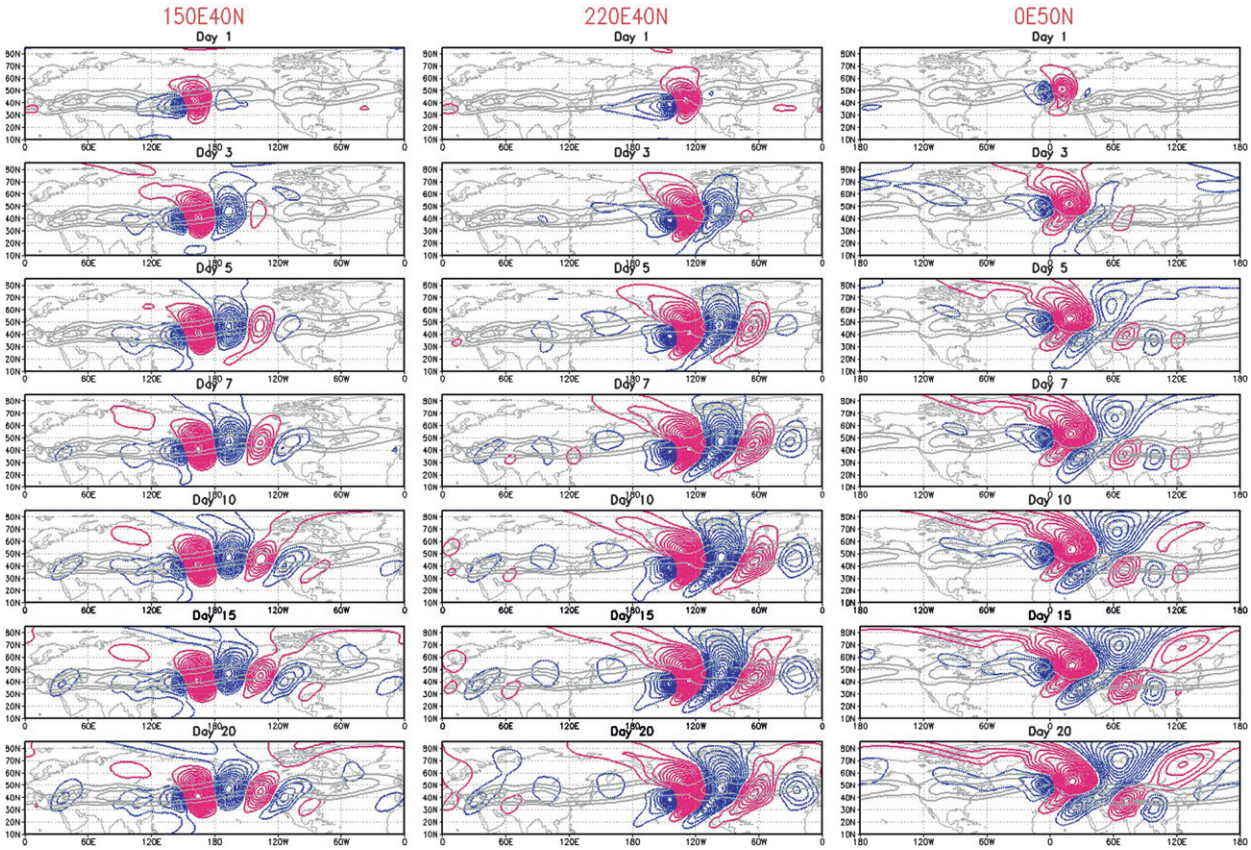

FIG. 11. (top to bottom) The time evolution of the response of the eddy v wind at $\sigma = 0.257$ to an idealized vorticity source at (left) 40°N, 150°E, (middle) 40°N, 220°E, and (right) 50°N, 0°. The results are from a stationary wave model with a three-dimensional JJA mean base state taken from MERRA for the period 1979–2010. See text for details of the forcing. Contour interval is 0.08 m s^{-1}. Note that the central longitude is 180° for the first two columns of plots, while it is 0° in the far right column of plots.

over Eurasia, with one branch moving north of the jet across Russia, while the other branch moves slightly south and remains largely embedded in the jet. The basic structure of this wave is quite similar to that of ROEF 1 (Fig. 3).

The above results are generally consistent with previous theoretical studies of boreal summer Rossby waves in the atmosphere. For example, Ambrizzi et al. (1995) summarized the boreal summer waveguides and preferred propagation patterns toward and away from the waveguides (e.g., their Fig. 17). The current results are generally consistent with the structures and wave paths found in that study, although the propagation of wave activity over Russia (found in the SWM and MERRA) is less prominent in their study.

We next address the forcing of the leading patterns (REOFs) found in MERRA within the context of the SWM. We begin by carrying out a series of forcing experiments using the idealized heating and vorticity sources described earlier. In one set, we introduce heat sources centered at every 10° longitude and 5° latitude to build up a collection of responses to heating over the Northern Hemisphere. In another set, we build up a collection of responses to vorticity sources over the Northern Hemisphere. Inner products are then formed between each of the upper-level eddy v responses and each of the 5 leading REOFs and plotted at the forcing location. The result (Fig. 12) gives an indication of those locations where forcing tends to produce a response that resembles one of the REOFs. We interpret the inner product patterns as the optimal forcing distributions for the REOFs. For example, the top panels of Fig. 12 show that heating over Europe generates a response that projects strongly onto REOF1, while heating over Russia (near 60°E) also produces a relatively strong response in REOF 1 but with opposite sign. In addition to forcing that is collocated with the region where the mature wave amplitude is largest, upstream heating along the southern part of the North American–Atlantic jet extending southeastward over Northern Africa also produces a response that projects onto REOF 1. Similar results are obtained for the response to vorticity sources (right top

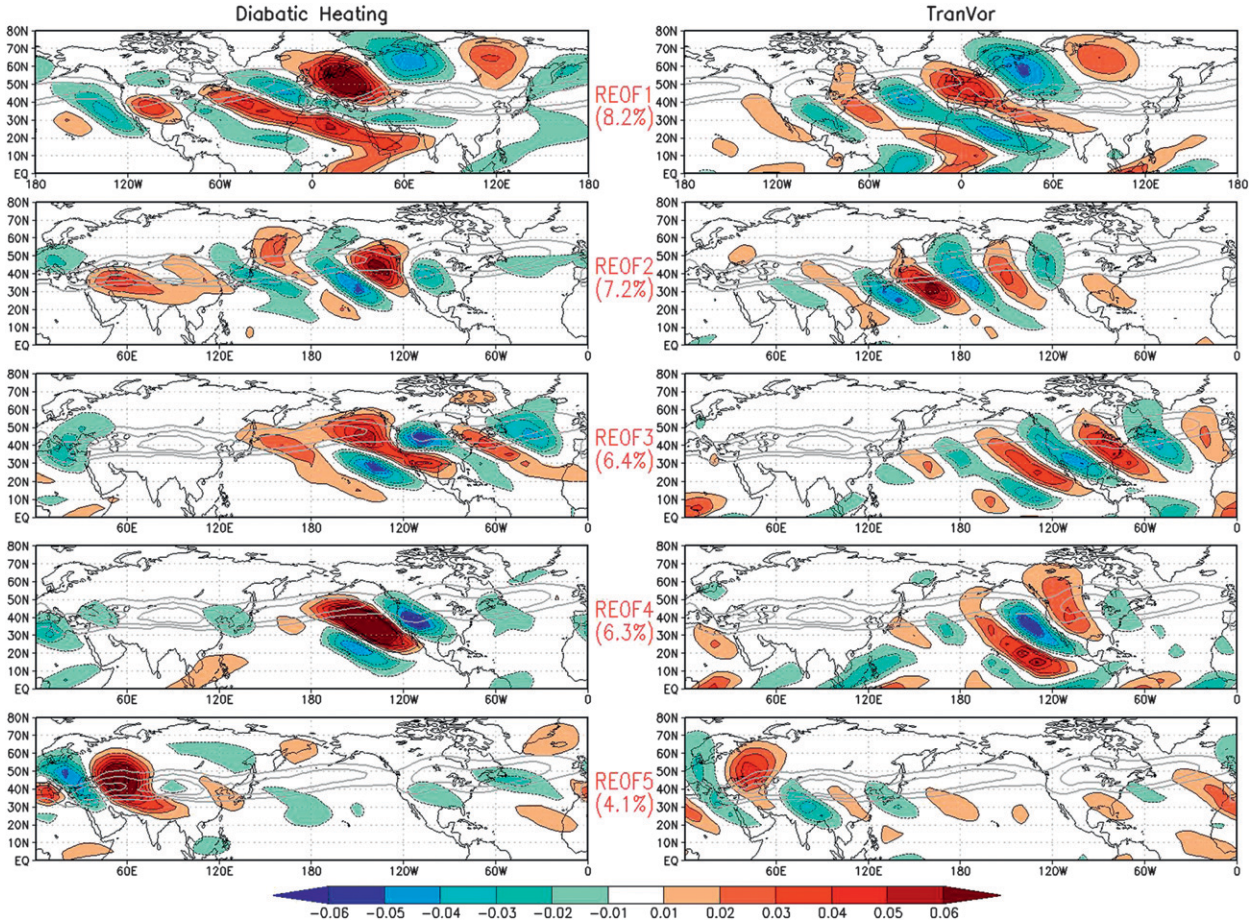

FIG. 12. The optimal forcing regions for (top to bottom) the 5 leading REOFs based on the stationary wave model results using a JJA 1979–2010 mean three-dimensional base state from MERRA. (left) The optimal patterns for the heating, and (right) the optimal patterns for vorticity. The patterns are computed as the inner product between the eddy v-wind response at $\sigma = 0.257$ to the forcing and the REOFs (see text for details). Units are arbitrary. Note that the central longitude in the plot for REOF 1 is 0°, while it is 180° for the others.

panel in Fig. 12), although in this case the v wind tends to be in quadrature with the forcing—consistent with a barotropic response.

The next set of panels (second from the top) in Fig. 12 shows that REOF 2 can be forced with heating or vorticity sources anywhere from Europe to western North America along the Asian/Pacific jet. The largest response in REOF 2 to heating occurs just off the west coast of North America, while the strongest response to vorticity forcing occurs just south of the jet in the western Pacific. REOF 3 (third row form the top in Fig. 12) is most readily forced (with both heating and vorticity sources) in a broad region extending from the eastern Pacific just south of the jet, across the United States and Mexico, into the North Atlantic.

REOF 4, in contrast to REOF 3, has a longitudinally more limited region of optimal forcing that is largely confined to the eastern Pacific. As already mentioned in the previous section, REOF 4 played an important role in the U.S. 1988 drought and 1993 flood. The forcing location in the eastern Pacific is consistent with some of the earlier work on drought in the central United States (e.g., Trenberth and Branstator 1992; Trenberth and Guillemot 1996; Mo et al. 1997). On the other hand, Chen and Newman (1998) suggest that the forcing for the June anomalies lies in the western North Pacific and Southeast Asia—a period (early spring) that is particularly conducive to cross-Pacific propagation of Rossby waves as discussed in Newman and Sardeshmukh (1998). They showed that the most sensitive area of forcing for producing a large response over the United States shifts from the east Pacific in late winter to the west Pacific by late spring, and that the amplitude of the forced response can potentially be larger in June than any other month of the year. Our SWM experiments with different basic states (not shown) also show that the June base state produces more robust wave propagation (compared with May and July) across the Pacific

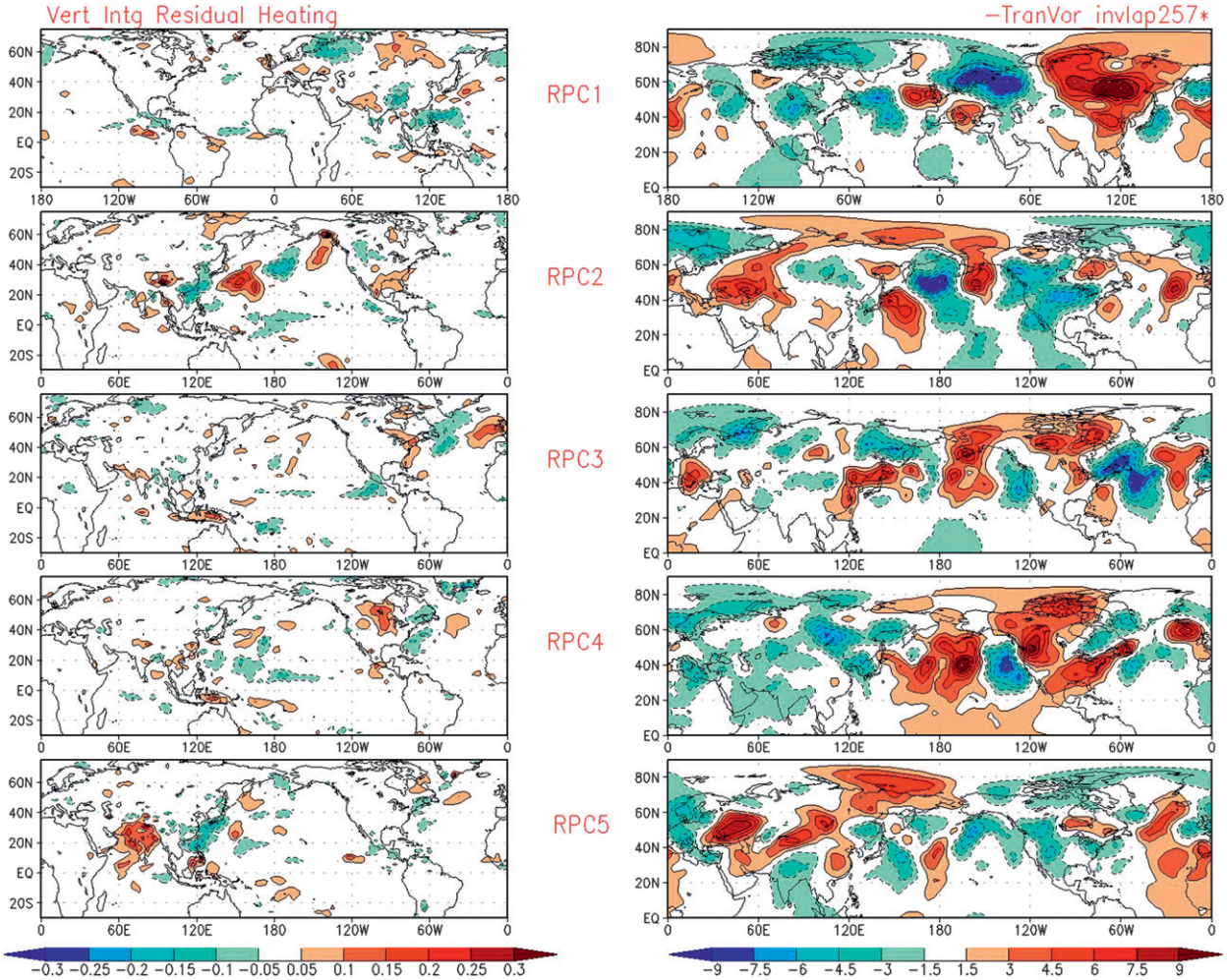

FIG. 13. (left) Vertically integrated heating and (right) eddy (zonal mean removed) transient vorticity forcing at $\sigma = 0.257$ estimated from MERRA associated with (top to bottom) each REOF. The results are based on a simple linear regression at each grid point in which the predictor is the REOF and the predictand is the subseasonal forcing. The results are plotted assuming one standard deviation in the RPCs. Units in the left panels are K day^{-1}. The transient vorticity forcing fields are smoothed by applying the inverse Laplacian (m^2 s^{-2}). Note that the central longitude in the plot for REOF 1 is 0°, while it is 180° for the others.

in response to forcing in the subtropical western Pacific. We also note that REOF 2 (the wave pattern extending across the Pacific) does exhibit some preference for June in that, of the 5 most extreme events (those exceeding 2 standard deviations in the subseasonal variability), three occurred in June, one in July, and one in August. Nevertheless, the pattern most relevant to the 1988 drought (REOF 3) is in our case more easily forced by heating or vorticity transients in the eastern North Pacific. We do find that prior to the development of REOF 4 in late May–early June of 1988, there is evidence for Rossby wave propagation across the Pacific during the first half of May that could set the stage (e.g., provide the vorticity forcing in the eastern Pacific) for the development of REOF 4 later that month. A similar mechanism was proposed by Wang et al. (2010), in the forcing of a June 2009 Rossby wave train in the North Pacific. Such an interpretation is also consistent with Liu et al. (1998) who found that western North Pacific heating appears to play a key role in forcing the anticyclonic anomaly that develops over the North Pacific in 1988. Finally, REOF 5 (bottom panels of Fig. 12) is most readily forced by heating in a region centered on 45°N and 55°E (just east of the Caspian Sea) and by vorticity sources just to the northwest of that region.

The optimal forcing patterns suggest that there are preferred regions of ''upstream'' forcing that might serve to initiate the waves. Other inferred forcing regions that are basically in phase with the regions of the largest wave response could potentially represent regions where local feedbacks are important for maintaining the wave. An example is REOF 1, where one could argue

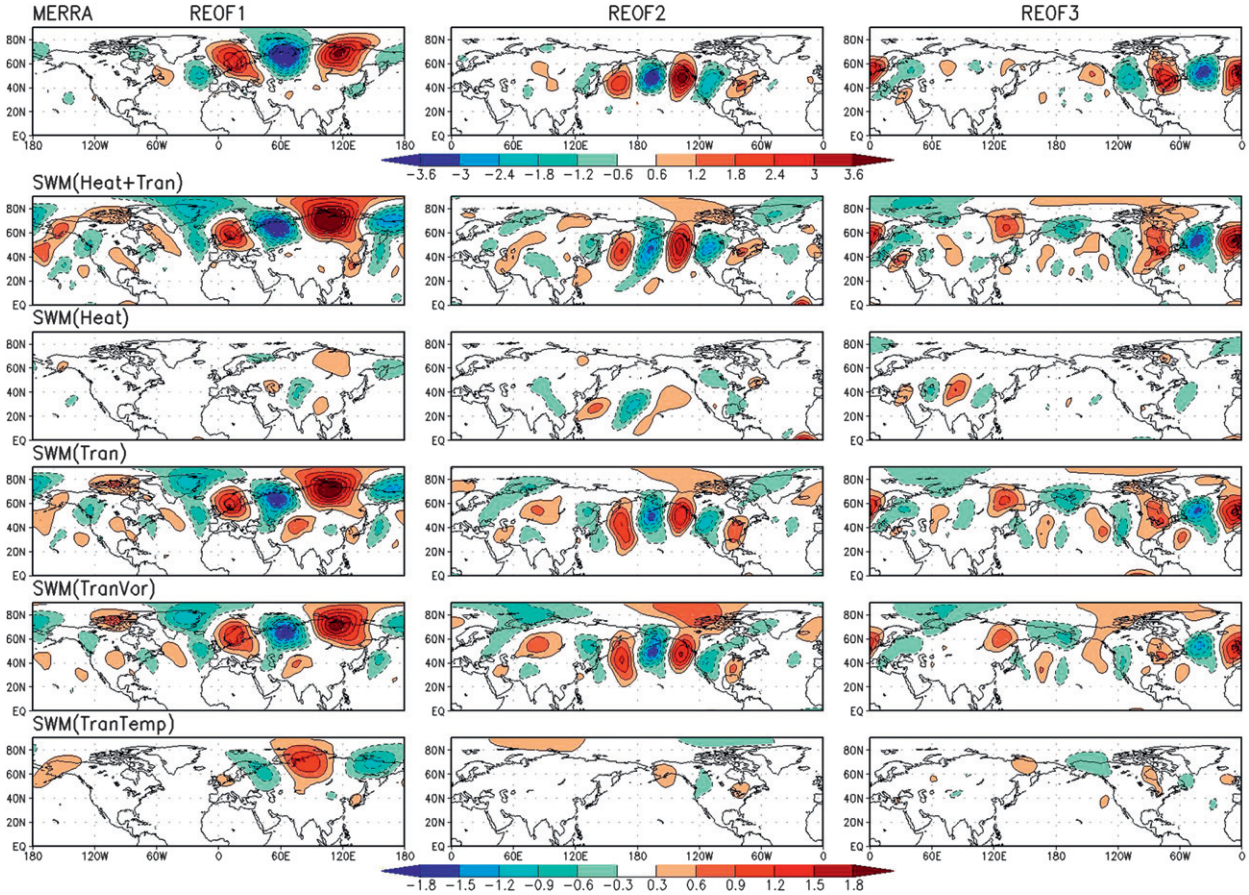

FIG. 14. (a) The first row is the subseasonal monthly JJA 250-hPa v-wind regressed against (left to right) the three leading REOFs, and plotted assuming one standard deviation in the REOFs. The remaining rows are the responses to the estimated forcing terms for the (left) first, (middle) second, and (right) third REOFs. The second from the top row is the response to the total forcing. The third row is the response to the heating. The fourth row shows the response to the total (temperature plus vorticity plus divergence) transient forcing. The fifth and sixth rows show the separate responses to the vorticity and temperature transients, respectively. Units: m s^{-1}. Note that the central longitude in the plot for REOF 1 is 0°, while it is 180° for the others. (b) As in (a), but for the (left) fourth and (right) fifth leading REOFs.

that while the wave could be initiated by (say vorticity) forcing somewhere upstream of the wave along the North Atlantic jet, once the wave is mature, local heating feedbacks over Eurasia could play an important role in helping to maintain the wave (e.g., Fischer et al. 2007). This is in contrast with REOF 4 where the primary forcing seems to be upstream of the wave over the eastern Pacific.

b. Response to forcing estimated from MERRA

Ting and Yu (1998) develop the equations for the nonlinear anomaly model that form the basis of the stationary wave model used here. The prognostic variables (vorticity, divergence, temperature, and log-surface pressure) are departures from the prescribed basic state (in our case the three-dimensional JJA mean from MERRA). The time mean quadratic transient terms act as forcing terms in each of the prognostic equations. Following Wang and Ting (1999), the leading adiabatic terms of the forcing are estimated from 3-hourly MERRA output on pressure levels as follows:

$$\mathrm{TF}_{\mathrm{vor}} = -\mathbf{\nabla} \cdot (\overline{V'\zeta'}), \tag{2a}$$

$$\mathrm{TF}_{\mathrm{div}} = \mathbf{k} \cdot \mathbf{\nabla} \times (\overline{V'\xi}) - \frac{1}{2}\nabla^2(\overline{V' \cdot V'}), \quad \text{and} \tag{2b}$$

$$\mathrm{TF}_{\mathrm{temp}} = -\left(\frac{p}{p_o}\right)^{R/c_p}\left[\mathbf{\nabla} \cdot (\overline{V'\theta'}) + \frac{\partial(\overline{\omega'\theta'})}{\partial p}\right], \tag{2c}$$

where ζ is the vorticity, V is the horizontal wind, p is pressure, ω is the pressure vertical velocity, and $\mathrm{TF}_{\mathrm{vor}}$, $\mathrm{TF}_{\mathrm{div}}$, and $\mathrm{TF}_{\mathrm{temp}}$ indicate that these are the transient forcing terms in the vorticity, divergence, and temperature

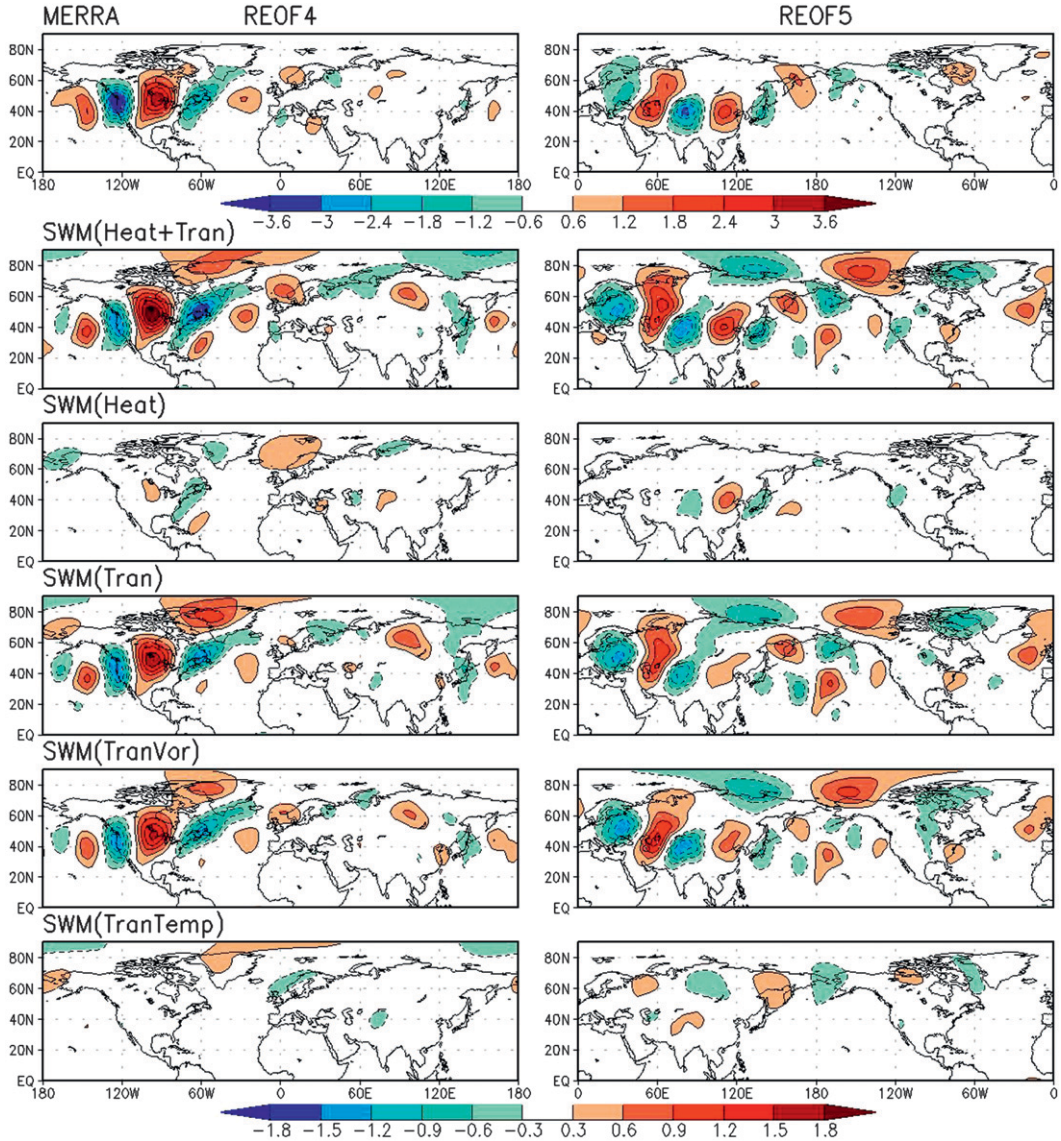

FIG. 14. (*Continued*)

equations, respectively. The overbar indicates a monthly mean, and the prime indicates a deviation from the monthly mean. The full form of the transient forcing terms can be found in Ting and Yu (1998). Also following Wang and Ting (1999), the total diabatic heating (Q) is estimated from MERRA as a residual of the temperature equations in pressure coordinates as

$$\overline{Q} = \frac{\partial \overline{T}}{\partial t} + \overline{\mathbf{V}} \cdot \nabla \overline{T} + \overline{\omega}\left(\frac{\partial \overline{T}}{\partial p} - \frac{R\overline{T}}{c_p p}\right) - \mathrm{TF}_{\mathrm{temp}}. \quad (3)$$

The above stationary wave forcings are then linearly interpolated onto the R30L14 resolution of the SWM. To examine the forcing associated with the REOFs, we compute the forcing at each grid point and for each summer month based on daily MERRA data for 1979–2010. The subseasonal monthly transient forcing and diabatic heating are then regressed against the normalized monthly subseasonal RPCs.

The results of the regression for the 5 leading REOFs are shown in Fig. 13 for the vertically integrated diabatic heating (left panels) and the vorticity forcing by transients in the upper troposphere (right panels). The heating fields (left panels) to a large extent resemble the correlations with the precipitation (e.g., Figs. 4 and 5). This is not surprising, and reflects the difficulties in separating the initial forcing from the response and feedbacks associated with the mature wave. The eddy

transient vorticity forcing fields are very noisy and for display purposes, they have been smoothed by applying an inverse Laplacian operator.[5] Again, the fields reflect the basic structures of the mature waves, although there are also some aspects of the idealized ''optimal'' forcing structures shown in Fig. 12 (right panels). For example, the forcing along the North Atlantic jet and over Europe resembles the structures in the optimal forcing for REOF1, and the forcing over the eastern North Pacific resembles those for REOF 2. In any event, we can assess the accuracy of the estimated forcing by using it to force the stationary wave model and determining whether it reproduces the REOFs.

Figure 14 shows the results of forcing the SWM with the above three-dimensional diabatic heating and transient eddy forcing fields associated with the 5 leading REOFs as determined from the linear regression. The strength of the forcing corresponds to one standard deviation in the predictors (the RPCs). The response to the transient divergence forcing is small in all cases and is not shown. In fact, the transient vorticity forcing dominates the response in all cases, with weaker contributions from the heating and transient temperature forcing terms. The small contribution from the heating to the forcing is (as noted above) likely an indication that the heating estimates represent a response to the wave rather than a forcing. This is also consistent with the relatively small precipitation variance explained by the leading REOFs (Fig. 6). Overall the SWM, when forced with the three-dimensional forcing terms estimated from MERRA, does a remarkably good job of reproducing the individual REOF structures, although the amplitude is about half that expected (the amplitude corresponding to 1 standard deviation of the REOFs). The reasons for this are unclear, though it may be that (2) underestimates the magnitude of the transient forcing terms.

In the case of REOF 1 (left panels of Fig. 14a), the temperature transients also play a significant role, with a response that is in quadrature with the response to the vorticity transients acting to shift the total response somewhat to the west. The heating in the eastern Pacific appears to play a significant role in the REOF 2 response (middle panels of Fig. 14a), although the response is largely out of phase with the response to the vorticity transients. The remaining leading REOFs (3–5) have only minor contributions from all but the transient vorticity forcing term. While overall, the SWM forced with the MERRA transients and heating reproduces the basic structure of the leading REOFs remarkably well, there are some differences—notably the results for REOF 5 (right panels of Fig. 14b), which show a much stronger amplitude at high latitudes (near 60°N) than is found in REOF 5. This is also true for the third and fourth REOFs—though less so.

5. Summary and conclusions

The results of this study show that stationary Rossby waves play an important role in boreal summer subseasonal variability, accounting for more than 30% (60%) of the monthly mean precipitation (surface temperature) variability over many regions of the extratropical land areas, including the U.S. northern Great Plains, parts of Canada, Europe, and Russia. The waves tend to develop within the mean jets and, within a few weeks, span much of the globe. A decomposition of the monthly mean 250-hPa meridional wind variability into REOFs highlights the regions where the Rossby waves tend to occur. The wave associated with the leading REOF appears to develop in the North Atlantic jet and then splits as it exits the jet, with most of the wave energy propagating north of the Eurasian jet across northern Europe and Russia, where it is a dominant contributor to monthly surface temperature and precipitation variability. The second REOF spans the globe from India to North America, while the third and fourth extend from the eastern Pacific to Europe—all three having important impacts on the hydroclimate of North America. The fifth REOF extends eastward from Europe across southern Eurasia, into the North Pacific.

The waves are at times (either as a subseasonal event or in combination with a seasonal mean component) major contributors to short-term climate extremes such as heat waves and flooding events. Examples include the 2003 European and 2010 Russian heat waves (REOF 1) and the June peak of the 1988 drought and the July peak of the 1993 flood over the United States (REOF 4). The significant projection of seasonal mean variability on the subseasonal REOFs is consistent with earlier work (Lau and Weng 2002; Lau et al. 2004; Ding and Wang 2005), which found that stationary Rossby waves play an important role on interannual time scales in the teleconnections that span from Eurasia to North America.

A stationary wave model, driven by localized heating or vorticity sources and using a climatological three-dimensional JJA base state, is able to reproduce some of the basic characteristics of the waves identified from MERRA. This includes the basic wave structures, wavelengths, and their near-circumglobal extent. A series of experiments, in which the SWM was forced with localized heating and vorticity sources, quantified the preferred regions of forcing of the leading REOFs. The forcing patterns are typified by wavelike structures with the largest

[5] The SWM is forced with the transient vorticity forcing with the zonal mean removed (the eddy component).

responses occurring when the forcing is just south of the jets and/or embedded in the developing wave; the latter forcing regions suggest that local feedbacks may be important.

A second set of experiments were carried out in which the SWM model was forced by MERRA estimates of the heating and transient forcing terms associated with each REOF. The responses to the forcing estimates show a remarkable agreement with the REOFs, indicating that the MERRA estimates of the forcing appear to be realistic. A key result is that the transient vorticity fluxes are by far the dominant forcing terms for the leading REOF wave structures, with diabatic heating and temperature transients playing a secondary role. These results are generally consistent with those of Liu et al. (1998), who found that transients played an important role in maintaining both the JJA 1993 and the April, May, June (AMJ) 1988 North American circulation anomalies, although at seasonal time scales they found that diabatic heating also played a role, especially during 1988. The importance of transient eddy forcing during the 1993 U.S. Midwest flood is further supported by Mo et al. (1995), who found that transient eddy feedback on the mean zonal flow played an important role in the development of the trough that remained locked on the lee side of the Rocky Mountains during that summer.

We found some limited evidence for a preference for the most extreme events to occur during June. This was limited to REOFs 1 (the wave extending from the eastern North Atlantic across Eurasia) and 2 (the wave spanning the North Pacific). In the case of REOF 2, this is consistent with Newman and Sardeshmukh (1998), who found that the seasonal changes in the shape and location of the Rossby waveguide favor a June response over the United States to forcing over the west Pacific. In the cast of REOF 1, the reasons for a June preference are not clear. Limited tests with the SWM (not shown) do not suggest large sensitivities of the response to forcing in the Atlantic jet to the annual cycle of the summer waveguide. In fact, as the wave energy associated with REOF 1 propagates out of the Atlantic jet exit region and across northern Russia it does so in a region of climatologically weak zonal winds. We have found some evidence, again based on SWM experiments, that an anomalous eastward extension of the Atlantic jet across northern Europe and Russia (such as that found during the months prior to the 2003 and the 2010 heat waves) does facilitate the development of the Eurasian Rossby wave.

While we have shown that stationary Rossby waves play an important role in subseasonal variability, and at times are major players in the development of short-term climate extremes, it is as yet unclear to what extent they are predictable. The important role of vorticity transients in forcing the waves would suggest that the predictability may be limited. A key issue here is the extent to which the seasonal means are primarily comprised of the statistical residual of the subseasonal variations, or whether other forcing (e.g., diabatic heating) and feedbacks (e.g., with soil moisture) contribute enough to significantly alter the variability and enhance the predictability at these time scales (e.g., as suggested by the shift in the centers of seasonal variability shown in Fig. 2). Slowly varying changes in the base state and associated changes in the waveguides (that could be linked to SST changes) may also play a role especially for some of the most extreme events such as the 2003 European or the 2010 Russian heat waves, or periods (e.g., during the 1993 floods) when they seem to contribute to the seasonal mean anomalies.

In any event, current GCMs appear to be deficient in reproducing aspects of the summer jet climatology that likely limit their ability to accurately simulate and predict the development of such Rossby waves (e.g., Hurrell et al. 2006). In addition to improving the models, it is possible that ensemble initialization schemes that take advantage of the identified preferred forcing patterns (e.g., Fig. 12) to better span the forecast uncertainty could produce greater skill than is achieved in current extended range forecasts.

Acknowledgments. Support for this project was provided by the NASA Modeling, Analysis and Prediction (MAP) Program, and the NOAA Climate Prediction Program for the Americas (CPPA).

REFERENCES

Adler, R. F., and Coauthors, 2003: The version 2 Global Precipitation Climatology Project (GPCP) monthly precipitation analysis (1979–present). *J. Hydrometeor.,* **4,** 1147–1167.

Ambrizzi, T., B. J. Hoskins, and H.-H. Hsu, 1995: Rossby wave propagation and teleconnection patterns in the austral winter. *J. Atmos. Sci.,* **52,** 3661–3672.

Atlas, R., N. Wolfson, and J. Terry, 1993: The effect of SST and soil moisture anomalies on GLA model simulations of the 1988 U.S. summer drought. *J. Climate,* **6,** 2034–2048.

Bloom, S., L. Takacs, A. DaSilva, and D. Ledvina, 1996: Data assimilation using incremental analysis updates. *Mon. Wea. Rev.,* **124,** 1256–1271.

Branstator, G., 2002: Circumglobal teleconnections, the jet stream waveguide, and the North Atlantic Oscillation. *J. Climate,* **15,** 1893–1910.

Carril, A. F., S. Gualdi, A. Cherchi, and A. Navarra, 2007: Heatwaves in Europe: Areas of homogeneous variability and links with the regional to large-scale atmospheric and SSTs anomalies. *Climate Dyn.,* **30,** 77–98, doi:10.1007/s00382-007-0274-5.

Chen, P., and M. Newman, 1998: Rossby wave propagation and the rapid development of upper-level anomalous anticyclones during the 1988 U.S. drought. *J. Climate,* **11,** 2491–2504.

Ding, Q., and B. Wang, 2005: Circumglobal teleconnection in the Northern Hemisphere summer. *J. Climate,* **18,** 3483–3505.

——, and ——, 2007: Intraseasonal teleconnection between the summer Eurasian wave train and the Indian monsoon. *J. Climate,* **20,** 3751–3767.

Dirmeyer, P. A., and K. L. Brubaker, 1999: Contrasting evaporative moisture sources during the drought of 1988 and the flood of 1993. *J. Geophys. Res.,* **104** (D16), 19 383–19 397.

Fischer, E. M., S. I. Seneviratne, P. L. Vidale, D. Lüthi, and C. Schär, 2007: Soil moisture–atmosphere interactions during the 2003 European summer heat wave. *J. Climate,* **20,** 5081–5099.

Held, I. M., M. Ting, and H. Wang, 2002: Northern winter stationary waves: Theory and modeling. *J. Climate,* **15,** 2125–2144.

Hoskins, B. J., and T. Ambrizzi, 1993: Rossby wave propagation on a realistic longitudinally varying flow. *J. Atmos. Sci.,* **50,** 1661–1671.

Hurrell, J. W., J. J. Hack, A. S. Phillips, J. Caron, and J. Yin, 2006: The dynamical simulation of the Community Atmosphere Model Version 3 (CAM3). *J. Climate,* **19,** 2162–2183.

Jiang, X., and N.-C. Lau, 2008: Intraseasonal teleconnection between North American and western North Pacific monsoons with 20-day time scale. *J. Climate,* **21,** 2664–2679.

Koster, R. D., M. J. Suarez, and M. Heiser, 2000: Variance and predictability of precipitation at seasonal-to-interannual timescales. *J. Hydrometeor.,* **1,** 26–46.

Lau, K.-M., and H.-Y. Weng, 2002: Recurrent teleconnection patterns linking summertime precipitation variability over East Asia and North America. *J. Meteor. Soc. Japan,* **80,** 1309–1324.

——, K.-M. Kim, and J.-Y. Lee, 2004: Interannual variability, global teleconnection and potential predictability associated with the Asian summer monsoon. *East Asian Monsoon,* C. P. Chang, Ed., World Scientific, 564 pp.

Liu, A. Z., M. Ting, and H. Wang, 1998: Maintenance of circulation anomalies during the 1988 drought and 1993 floods over the United States. *J. Atmos. Sci.,* **55,** 2810–2832.

Lyon, B., and R. M. Dole, 1995: A diagnostic comparison of the 1980 and 1988 U. S. summer heat wave droughts. *J. Climate,* **8,** 1658–1675.

Mitchell, T. D., and P. D. Jones, 2005: An improved method of constructing a database of monthly climate observations and associated high-resolution grids. *Int. J. Climatol.,* **25,** 693–712.

Mo, K. C., J. Nogues-Paegle, and J. Paegle, 1995: Physical mechanisms of the 1993 summer floods. *J. Atmos. Sci.,* **52,** 879–895.

——, J. N. Paegle, and R. W. Higgins, 1997: Atmospheric processes associated with summer floods and droughts in the central United States. *J. Climate,* **10,** 3028–3046.

Namias, J., 1983: Some causes of United States drought. *J. Climate Appl. Meteor.,* **22,** 30–39.

——, 1991: Spring and summer 1988 drought over the contiguous United States—Causes and prediction. *J. Climate,* **4,** 54–65.

Newman, M., and P. D. Sardeshmukh, 1998: The impact of the annual cycle on the North Pacific/North American response to remote low-frequency forcing. *J. Atmos. Sci.,* **55,** 1336–1353.

Oppenheim, A. V., and R. W. Schafer, 1975: *Digital Signal Processing*. Prentice-Hall, 585 pp.

Parker, M. D., and R. H. Johnson, 2000: Organizational modes of midlatitude mesoscale convective systems. *Mon. Wea. Rev.,* **128,** 3413–3436.

Richman, M. B., 1986: Rotation of principal components. *Int. J. Climatol.,* **6,** 293–335.

Rienecker, M. M., and Coauthors, 2008: The GEOS-5 data assimilation system—Documentation of versions 5.0.1, 5.1.0, and 5.2.0. NASA Tech. Rep. Series on Global Modeling and Data Assimilation, NASA/TM-2007-104606, Vol. 27, 95 pp.

——, and Coauthors, 2011: MERRA—NASA's Modern-Era Retrospective Analysis for Research and Applications. *J. Climate,* **24,** 3624–3648.

Ting, M. F., and L. Yu, 1998: Steady response to tropical heating in wavy linear and nonlinear baroclinic models. *J. Atmos. Sci.,* **55,** 3565–3582.

——, H. L. Wang, and L. H. Yu, 2001: Nonlinear stationary wave maintenance and seasonal cycle in the GFDL R30 GCM. *J. Atmos. Sci.,* **58,** 2331–2354.

Trenberth, K. E., and G. W. Branstator, 1992: Issues in establishing causes of the 1988 drought over North America. *J. Climate,* **5,** 159–172.

——, and C. J. Guillemot, 1996: Physical processes involved in the 1988 drought and 1993 floods in North America. *J. Climate,* **9,** 1288–1298.

Wang, H., and M. Ting, 1999: Seasonal cycle of the climatological stationary waves in the NCEP–NCAR reanalysis. *J. Atmos. Sci.,* **56,** 3892–3919.

Wang, S.-Y., L. E. Hipps, R. R. Gillies, X. Jiang, and A. L. Moller, 2010: Circumglobal teleconnection and early summer rainfall in the U.S. Intermountain West. *Theor. Appl. Climatol.,* **102,** 245–252.